CrossMark

ORIGINAL PAPER

Effect of Thermal Cycling on Compatibility in CO_2 for Concentrated Solar Power Applications

Robert G. Brese[1,2] · **James R. Keiser**[1] · **Bruce A. Pint**[1]

Abstract As a first step in evaluating materials for a concentrated solar power (CSP), supercritical CO_2 Brayton cycle, experiments are being conducted to simulate the daily operating cycle using 10-h thermal cycles in 1 bar CO_2 at 700–800 °C. After 1000-h exposures, the mass gains for commercial Ni-base alloys 740H, 282, 625 and Fe-base alloy 25 were relatively low with correspondingly thin reaction products. At 800 °C, similar reaction products were obtained for thermal cycling in CO_2 and dry air, which also could simulate the outside of the primary heat exchanger. In addition, 500-h cycles were conducted at 750 °C, which showed slightly higher mass gains than the 10-h cycles. In general, there were no indications of internal carburization for these four alloys after 1000 h and the measured rate constants are sufficiently low to meet the 30-year CSP lifetime goal.

✉ Robert G. Brese
breserg@ornl.gov

✉ Bruce A. Pint
keiserjr@ornl.gov

James R. Keiser
pintba@ornl.gov

[1] Materials Science and Technology Division, Oak Ridge National Laboratory, 1 Bethel Valley Rd, Oak Ridge, TN 37831, USA

[2] University of Tennessee, Knoxville, TN 37996, USA

Introduction

There is considerable interest in the use of supercritical CO$_2$ (sCO$_2$) for power generation applications including nuclear, fossil and concentrated solar power (CSP) [1–3]. The use of a sCO$_2$ Brayton cycle operating at temperatures greater than 700 °C has the potential to create efficiencies greater than 50% [4]. Initial work above 700 °C in sCO$_2$ has shown relatively low reaction rates for relevant Ni-base structural alloys [5–8]. A significant concern is the possible internal carburization that primarily has been seen for Fe-base alloys in CO$_2$ [9–13]. A unique aspect of the CSP application is the daily thermal cycling, which has been briefly studied for CSP air Brayton cycles [14, 15]. The current project has a goal of studying the long-term behavior of four commercial candidate structural alloys (Inconel 740H, Haynes 282, Sanicro 25 and alloy 625) in CO$_2$/sCO$_2$ in order to develop a CSP-relevant lifetime model. Long-term testing at 700–800 °C is in progress at 1 and 300 bar. The 1 bar work was included in order to conduct 10-h thermal cycling, which is not feasible in a 300 bar autoclave. The current results are for the first set of specimens removed after 1000 h (i.e., 100, 10-h cycles) at 700–800 °C. Comparisons are made with similar specimens thermally cycled in dry air at 800 °C and 500-h cycles in CO$_2$ at 750 °C.

Procedure

The chemical compositions of the four commercial alloys selected for testing in this study are shown in Table 1. Coupons (∼10 × 20 × 1.5 mm) were polished to a 600 grit finish and ultrasonically cleaned in acetone and methanol prior to exposure. For 10-h cycles, samples were hung from alumina rods with platinum wire and exposed in automated cyclic rigs [16] for 10 h in the hot zone followed by 10-min cooling in laboratory air to <30 °C after being automatically pulled from the furnace. Exposures at 700, 750 and 800 °C were conducted in industrial grade (IG) CO$_2$, with <50 ppm O$_2$ <32 ppm H$_2$O, and at 800 °C in dry air. Gas flow rates were ∼100 cc/min or ∼0.1 cm/s flow rate. For 500-h cycles, the specimens were placed in an alumina boat in an alumina reaction tube with end caps. The specimens were

Table 1 Alloy composition in mass% measured by inductively coupled plasma and combustion analyses

Alloy	Fe	Ni	Cr	Al	Co	Mo	Nb	Ti	Mn	Si	W	Other
25	42.6	25.4	22.3	0.03	1.5	0.2	0.5	0.02	0.5	0.2	3.5	3.0Cu, 0.2N
282	0.2	57.1	19.6	1.6	10.6	8.6	<	2.2	0.02	0.04	0.01	
740H	0.1	49.7	24.5	1.4	20.6	0.3	1.5	1.4	0.3	0.2	<	
625	4.0	61.0	21.7	0.12	0.1	8.8	3.5	0.2	0.2	0.2	0.06	0.09Cu

< is less than 0.002%

heated in argon to 750 °C over 4 h to minimize oxidation of the sample prior to exposure to CO_2, held for 500 h in industrial grade CO_2 and cooled in argon to room temperature. Specimens were weighed using a Mettler Toledo XP205 balance with an accuracy of $\sim \pm 0.04$ mg or 0.01 mg/cm^2. Mass change was measured every 160 h (16 cycles) in the cyclic tests. After exposure, samples were copper plated before being sectioned and mounted for light microscopy. Specimens were etched using aqua regia to measure internal oxidation. Both oxide thickness and internal oxidation were measured using image analysis software with >50 measurements taken for each specimen.

Results

Figure 1 shows the specific mass gain versus time for each of the four alloys investigated in 10-h cycles in 1 bar CO_2 at 700, 750 and 800 °C. Two specimens of each alloy were exposed at each temperature, and the mass changes were small at 700 and 750 °C with some scatter in behavior because of the low values. More uniform parabolic-type behavior was observed at 800 °C. The mass gain was unexpectedly low for the alloy 625 specimens, particularly at 800 °C. Higher mass gain was expected for the alloy 282 specimens in this temperature range due to the internal oxidation of Ti and Al [6, 8, 17]. Polished cross sections after 1000-h exposures at each temperature are shown in Fig. 2. In general, thin protective scales were observed in all cases. The internal oxidation for alloys 282 and 740 was clear at 750 and, at 800 °C, the internal oxidation increased significantly for both alloys. Alloys 625 and 25 contain much lower levels of Al and Ti (Table 1) and thus do not show signs of internal oxidation. The scale was slightly thicker on alloy 25 at 800 °C.

Figure 3 shows box and whisker plots for the scale thickness of the specimens shown in Fig. 2 with the box marking the 25%, median and 75% values measured and the whiskers showing the minimum and maximum values measured. All of the alloy specimens showed thin oxides with little variation in the median values at 700 and 750 °C. At 800 °C, 625 continued to form a very thin oxide, consistent with the mass change data in Fig. 1. Figure 4 shows box and whisker plots for the internal oxidation of the specimens after etching. Deeper internal oxidation can be seen in 740 and 282 specimens, especially at 750 and 800 °C.

In order to better understand the performance of these alloys in CO_2, a 10-h cyclic test was conducted in dry air at 800 °C and the mass change data are compared to the CO_2 data in Fig. 5. The mass gains were similar in both environments. Figure 6 shows that the oxide microstructures were similar in air with the oxide thickness measurements shown in Fig. 3c and the internal oxidation measurements in Fig. 4c. Particularly for the alloy 625 specimens, the oxide was slightly thicker in dry air compared to CO_2 after 100, 10-h cycles. For the other alloys, the oxide thickness and depth of internal oxidation were similar.

To better understand the effect of cycling, 500-h cycles also were conducted at 750 °C in 1 bar CO_2. Figure 7 compares the mass change data at 750 °C in 10- and 500-h cycles. For the 500-h cycle exposures, the average of eight specimens being
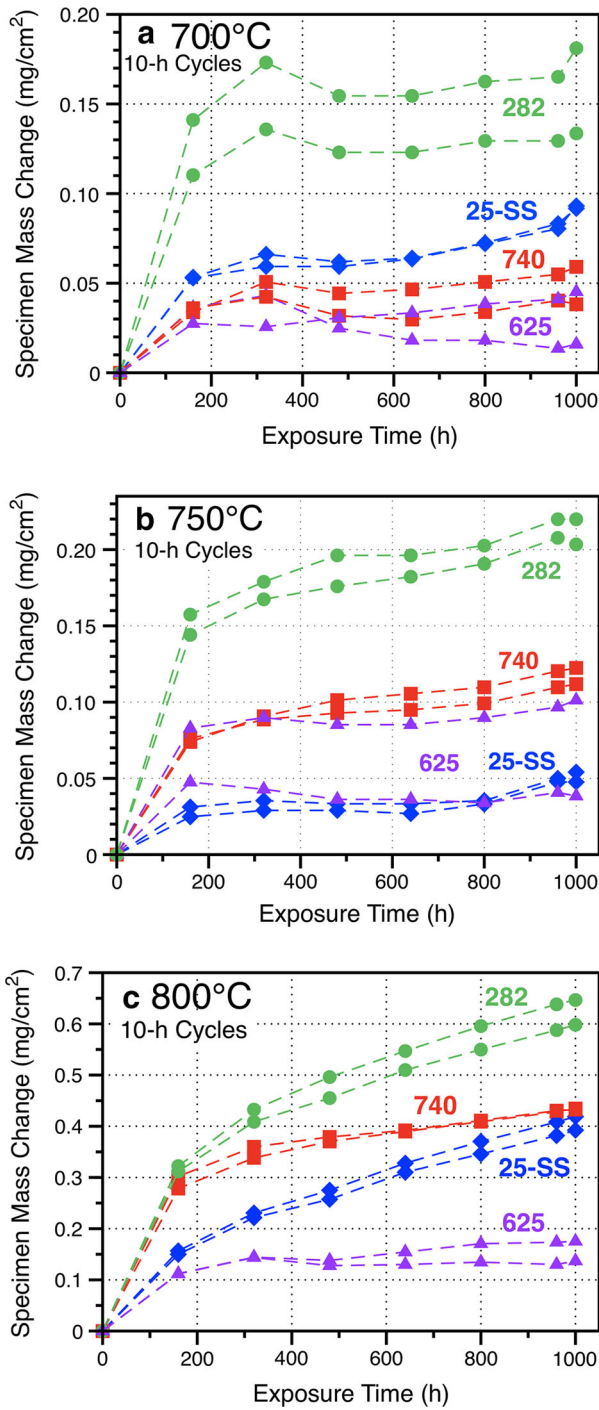
◄**Fig. 1** Specimen mass gain versus exposure time up to 1000 h for all four alloys at 700 °C (**a**), 750 °C (**b**) and 800 °C (**c**)
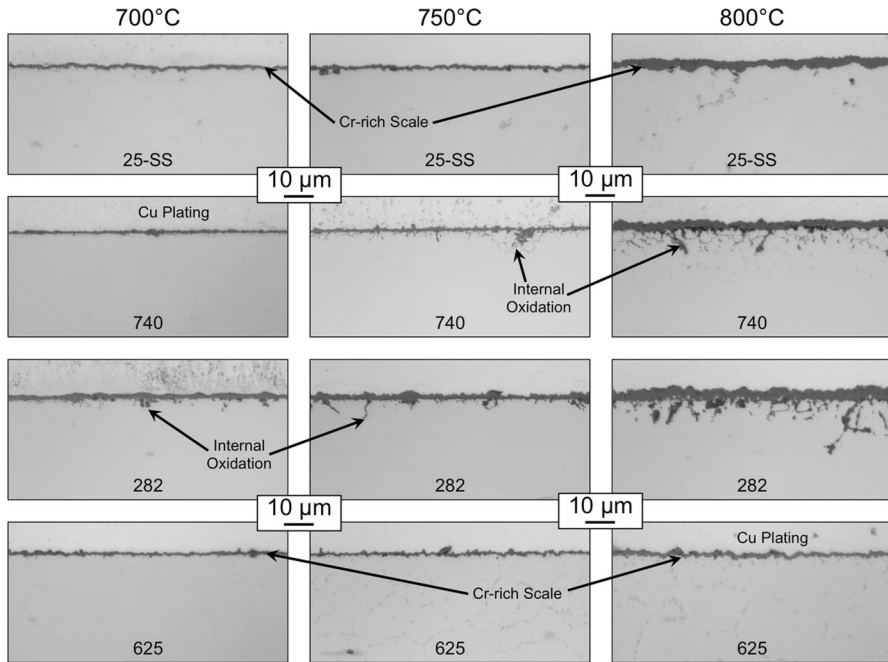

Fig. 2 Light microscopy of the four alloys after 10-h cycles for 1000 h in 1 bar industrial grade CO_2

exposed is shown. The additional specimens are being continued to longer exposure times. The mass gains were slightly higher in the 500-h cycle experiments, and these experiments have included exposures up to 1500 h. One specimen of each alloy was stopped after 1000 h, and Fig. 8 shows the oxides formed. The oxide measurements are shown in Fig. 3b along with the internal oxidation measurements in Fig. 4b. The median oxide thickness values were all slightly larger after 1000 h in the 500-h cycles compared to the values in 10-h cycles. An oxide nodule on the alloy 25-SS specimen skewed the maximum value for that specimen, Fig. 3b.

The oxidation kinetics were assumed to be parabolic, and the measured rate constants are shown in Fig. 9, calculated by plotting the mass change versus the square root of time, then squaring the linear fit of the data as described by Pieraggi [18]. For alloy 625, both specimens at 700 °C and one at 750 °C showed a mass loss after an initial mass gain and a rate was not fit. Tables 2 and 3 compare the rates measured at 800 °C in CO_2 and air and at 750 °C in 10- and 500-h cycles, respectively. The rates were slightly lower in air at 800 °C and higher in 500-h cycles at 750 °C.
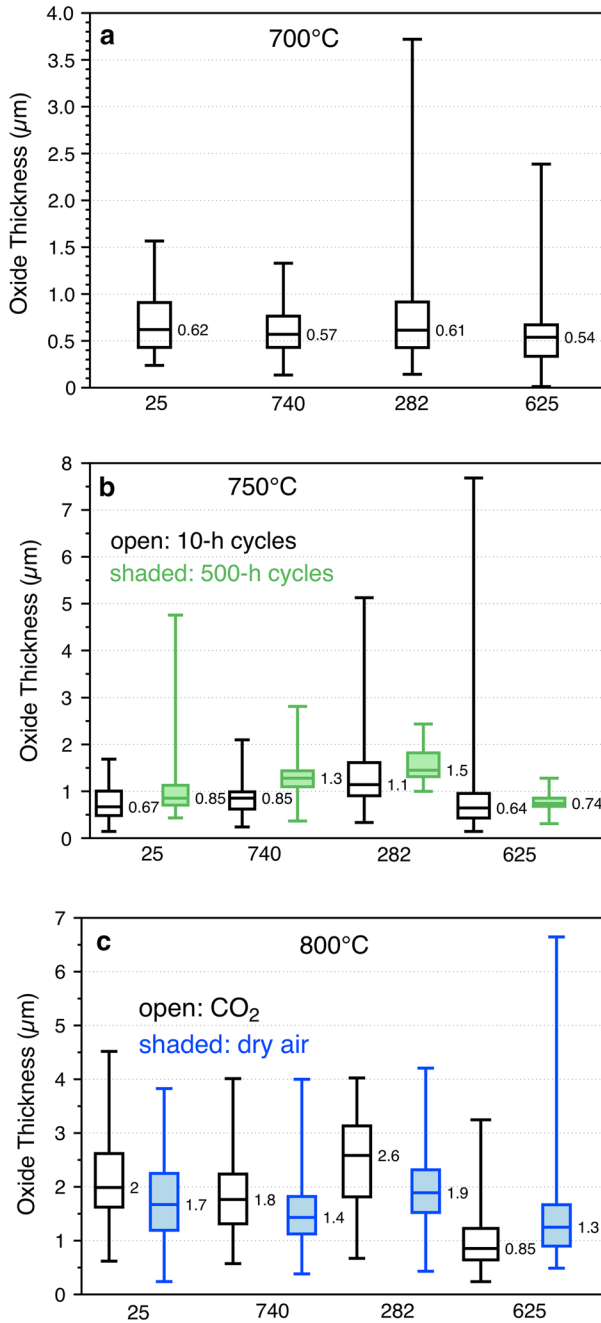
Fig. 3 Box and whisker plots of oxide thickness of samples after 1000-h exposures in 10-h cycles in 1 bar CO_2 at **a** 700 °C, **b** 750 °C and **c** 800 °C. At 750 °C, data are shown for 500-h cycles in CO_2 and at 800 °C in 10-h cycles in dry air
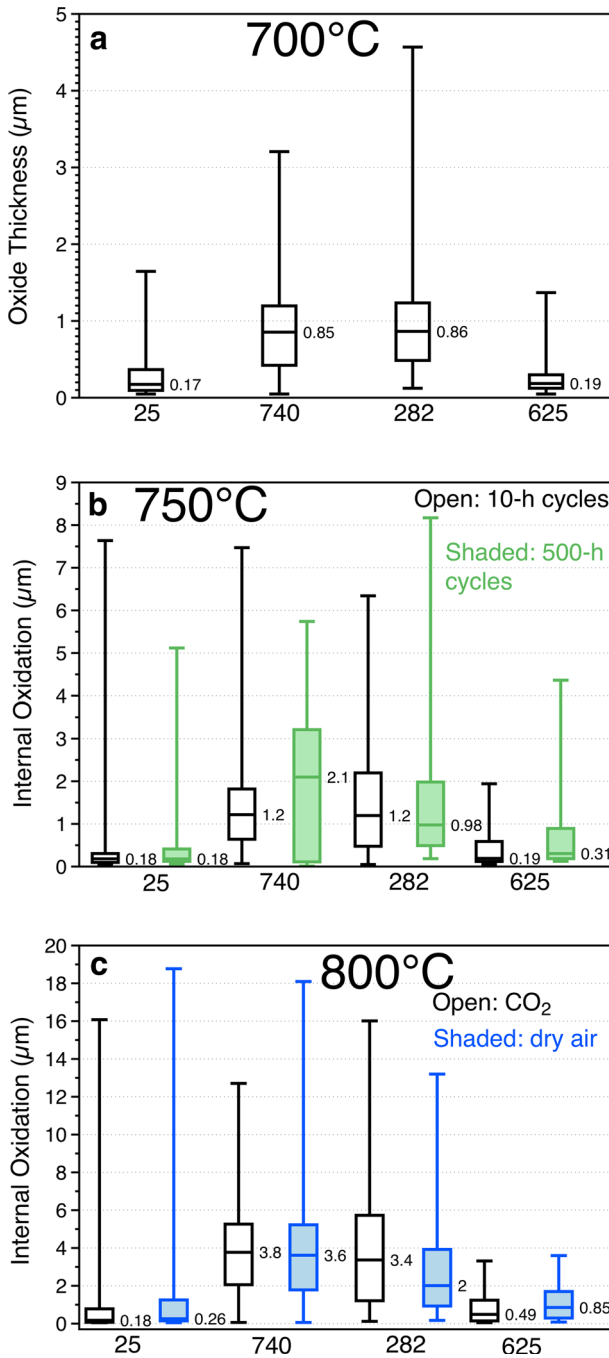
Fig. 4 Box and whisker plots of internal oxidation of etched cross sections after 1000-h exposures in 10-h cycles in 1 bar CO_2 at **a** 700 °C, **b** 750 °C and **c** 800 °C. At 750 °C, data are shown for 500-h cycles in CO_2 and at 800 °C in 10-h cycles in dry air
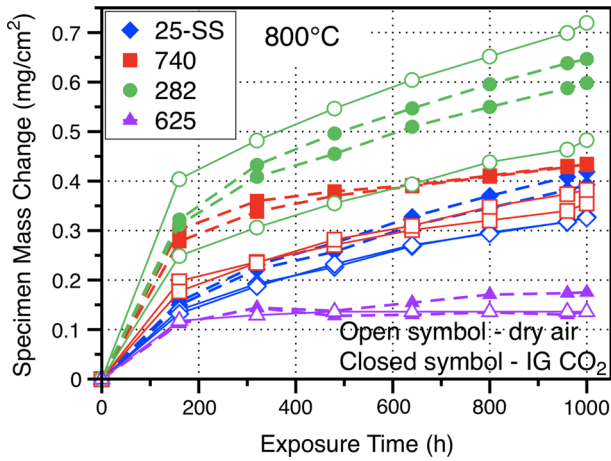
Fig. 5 Specimen mass gain versus exposure time for samples tested in dry air (*open symbols*) and CO_2 (*closed symbols*) at 800 °C
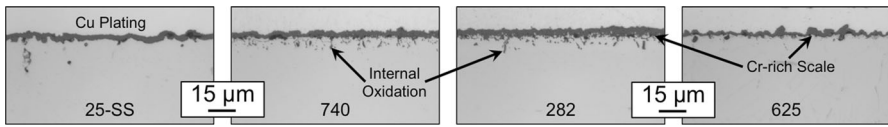

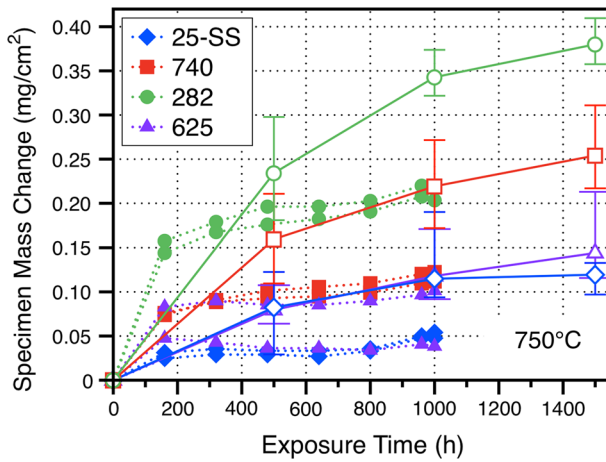**Fig. 6** Light microscopy of the four alloys after 10-h cycles for 1000 h in dry air at 800 °C

Fig. 7 Specimen mass gain of samples exposed in 1 bar CO_2 at 750 °C with 10-h (*closed symbols*) and 500-h cycles (*open symbols*). For the 500-h cycles, the average of eight specimens is shown including one standard deviation
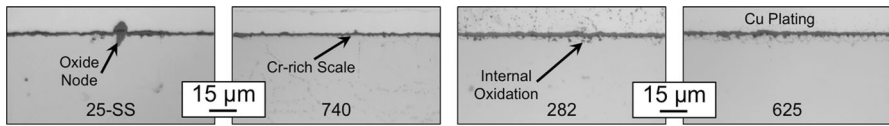
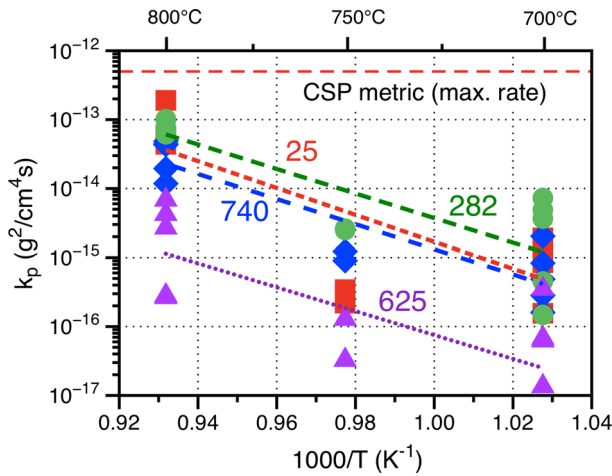**Fig. 8** Light microscopy of the four alloys after two 500-h cycles in 1 bar industrial grade CO_2

Fig. 9 Arrhenius plot of the parabolic rate constants (kp) for each individual sample in the 10-h CO_2 cycles. The rates for all four alloys are under the target metric for the CSP application of 5×10^{-13} g cm^{-4} s^{-1}. For comparison, the rates in air at 800 °C and in 500-h cycles in CO_2 are shown

Table 2 Comparison of the average parabolic rate constant (g^2 cm^{-4} s^{-1}) after exposure in dry air, and CO_2 using 10-h cycles at 800 °C

Alloy	Air	CO_2
282	5.8×10^{-14}	7.4×10^{-14}
740	2.5×10^{-14}	3.8×10^{-14}
25-SS	2.8×10^{-14}	5.2×10^{-14}
625	2.0×10^{-16}	1.5×10^{-15}

Table 3 Comparison of the average parabolic rate constant (g^2 cm^{-4} s^{-1}) after exposure in CO_2 at 750 °C using 10- and 500-h cycles

Alloy	500 h Cycles	10 h Cycles
282	2.4×10^{-14}	2.6×10^{-15}
740	1.2×10^{-14}	1.2×10^{-15}
25-SS	1.9×10^{-15}	3.1×10^{-16}
625	4.7×10^{-15}	1.0×10^{-16}

Discussion

In general, the measured corrosion rates were low in these experiments, Fig. 9, well below the rate constant goal of 5×10^{-13} g/cm^{4}s, which would form <100 μm of oxide scale in 100,000 h or ∼30 years of CSP operation. Some of the scatter in Fig. 1a, b can be associated with the low mass gains near the limit of the measurement procedure. The 625 and Fe-base 25 specimens, while having low overall growth rates, showed higher growth rates in CO_2 compared to air, Table 2. The experiment in air was used to understand the effect of CO_2 but is also relevant for the CSP application where the solar receiver (primary heat exchanger) could have CO_2 on the inside of tubes and air on the outside at slightly higher temperatures. Perhaps as high as 800 °C to have a turbine inlet temperature >700 °C, particularly if thermal storage is employed. Comparing the growth rates of the samples exposed in 10- and 500-h cycles at 750 °C showed that the growth rates after exposure in 500-h cycles were higher, Table 3 and Fig. 9. These could be attributed to scale spallation. However, these relatively thin scales are unlikely to spall significantly and no evidence of scale spallation was observed. Longer exposures to 4000 h that are currently in progress will help to differentiate the cycle frequency differences and refine the kinetic rates measured. The difference could also be due to the experiments being conducted in different furnaces. The temperature is much easier to monitor and control in a horizontal three-zone furnace than in the cyclic rigs, where each specimen is at a different location in a vertical tube.

Figure 9 also shows the Arrhenius fit of the parabolic rate constants. All of the alloys had a similar activation energy, except for alloy 625, which formed thinner scales, particularly at 800 °C. Longer experiments also will help to refine the rate calculations, which were somewhat scattered due to the low mass gains at these temperatures. In the 10-h cycle tests performed in CO_2, the rate constants calculated at 750 °C were lower than the values predicted by the Arrhenius fit. Since all three experiments were conducted in different cyclic rigs, a possible explanation is that the temperature in the 750 °C experiment was lower than expected resulting in the low mass gains observed.

The oxygen partial pressure in IG CO_2 is likely dictated by any O_2 impurities but even in pure CO_2 there is a sufficient oxygen partial pressure to form all of the major Fe, Ni and Cr oxides. However, the formation of Cr-rich oxides is relatively slow at these temperatures, Fig. 9. The main concern for the CO_2 environment is internal carburization. However, it has been extremely difficult to identify any internal carburization by scanning electron microscopy/energy-dispersive or wave length-dispersive spectroscopy. The internal oxidation values in air and CO_2 appeared quite similar at 800 °C, Fig. 4c. Again, longer exposures may help to differentiate behavior. Furthermore, the specimens were measured after etching. Figure 10 provides examples of the specimens after etching where the precipitates were highlighted along with the γ' depletion zone in 740H and 282. Figure 11 shows examples where the median depth values typically increased after etching.
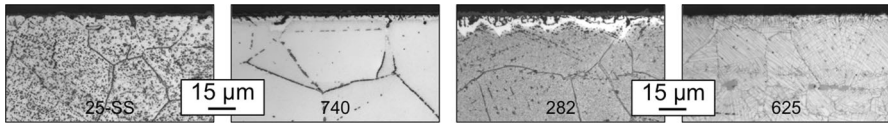
Fig. 10 Light microscopy of each alloy from the 10-h cycle tests in CO_2 at 750 °C after being etched with aqua regia
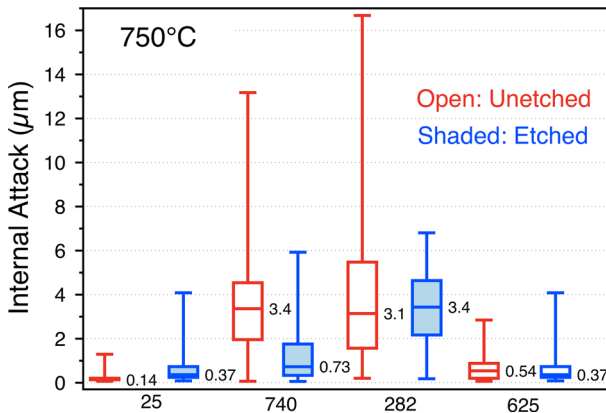

Fig. 11 Comparison of internal attack measurements before and after being etched

Because of the thin reaction products, higher resolution characterization is needed but currently there are no signs of any significant internal carburization after 1000 h in 1 bar IG CO_2. Comparisons of Fe- and Ni-base alloys have indicated more C ingress in Fe-base alloys [19], and it has been suggested that the lower C solubility in Ni-base alloys makes internal carburization less likely [7]. There is some concern about Fe-base alloy 25 being more susceptible to internal carburization; however, Fe-base alloys represent a less expensive alternative to Ni-base alloys for this application. For Fe-base alloy 25, very thin reaction products were observed at 700 and 750 °C in 10-h cycles. However, an oxide nodule was observed in the 500-h cycles (Fig. 3b) and the slightly thicker scale formed in CO_2 at 800 °C will be further characterized to determine their composition. Higher oxidation rates and deeper internal oxidation were observed for the precipitation-strengthened alloys, 740H and 282, particularly at 800 °C. However, these alloys are significantly stronger than conventional solid solution-strengthened Ni-base alloys like 625 and are the most likely candidates for 750–800 °C applications [20, 21].

Another reason to conduct the 500-h cycles in 1 bar CO_2 is that the next phase of this testing will include 300 bar sCO_2 experiments at 700–800 °C using 500-h cycles and the 500-h 1 bar experiment will help isolate the effects of cycling and CO_2 pressure on performance. If CO_2 pressure does not strongly affect behavior, as has been shown in other studies [8, 11], then there is less need to conduct high-pressure autoclave experiments.

Conclusions

Four commercial structural alloys were investigated for their use in a supercritical CO_2 Brayton cycle CSP system. In this initial phase of the study, coupons were exposed for 1000 h in 10- and 500-h cyclic exposures in 1 bar CO_2 at 700–800 °C. The high-strength precipitation-strengthened alloys 740 and 282 showed increased internal oxidation due to the higher Al and Ti contents in these alloys. A comparison experiment at 800 °C in dry air showed similar mass gains and reaction products as CO_2. This initial characterization showed no indication of internal carburization under these conditions. The reaction rates were slightly higher at 750 °C in 500-h cycles. All of the measured reaction rates were low and suggest these alloys have a good chance of meeting the 30-year CSP durability goal for this application based on oxidation resistance. Longer exposures in these experiments at 1 bar and complementary exposures at 300 bar will help to develop and verify a lifetime model for this application.

References

1. V. Dostal, P. Hejzlar and M. J. Driscoll, *Nuclear Technology* **154**, 2006 (283).
2. R. Chacartegui, J. M. Muñoz De Escalona, D. Sánchez, B. Monje and T. Sánchez, *Applied Thermal Engineering* **31**, 2011 (5).
3. V. Cheang, R. Hedderwick, and C. McGregor, *Solar Energy*, **113**, 2015 (199–211).
4. E. G. Feher, *Energy Conversion* **8**, 1968 (85).
5. C. Oh, T. Lillo, W. Windes, T. Totemeier, B. Ward, R. Moore, and R. Barner, Idaho National Laboratory Report INL/EXT-06-01271, Idaho Falls, ID, 2006.
6. B. A. Pint and J. R. Keiser, *JOM* **67**, 2015 (2615–2620).
7. R. I. Olivares, D. J. Young, P. Marvig and W. Stein, *Oxidation of Metals* **84**, 2015 (585).
8. B. A. Pint, R. G. Brese, and J. R. Keiser, *Materials and Corrosion* **68**, 2017 (151–158).
9. H. E. McCoy, *Corrosion* **21**, 1965 (84).
10. F. Rouillard, G. Moine, M. Tabrant and J. C. Ruiz, *Oxidation of Metals* **77**, 2012 (57).
11. T. Furukawa, Y. Inagaki and M. Aritomi, *Progress in Nuclear Energy* **53**, 2011 (1050).
12. V. Firouzdor, K. Sridharan, G. Cao, M. Anderson and T. R. Allen, *Corrosion Science* **69**, 2013 (281).
13. T. D. Nguyen, J. Q. Zhang and D. J. Young, *Materials at High Temperatures* **32**, 2015 (16).
14. B. A. Pint, *Material Science Forum* **696**, 2011 (57).
15. B. A. Pint, B. N. Anderson, W. J. Matthews, C. Waldhelm, and W. Treece, ASME Paper #GT2013-94939, presented at the International Gas Turbine & Aeroengine Congress & Exhibition, San Antonio, TX, June, 3–7, 2013.
16. B. A. Pint, P. F. Tortorelli and I. G. Wright, *Oxidation of Metals* **58**, 2002 (73).
17. E. Essuman, L. R. Walker, P. J. Maziasz and B. A. Pint, *Materials Science and Technology* **29**, 2013 (822–827).
18. B. Pieraggi, *Oxidation of Metals* **27**, 1987 (177).
19. H. J. Lee, H. Kim, S. H. Kim and C. Jang, *Corrosion Science* **99**, 2015 (227–239).
20. J. P. Shingledecker and G. M. Pharr, *Journal of Materials Engineering Performance* **22**, 2013 (454–462).
21. L. M. Pike, *Superalloys 2008*, eds. R. C. Reed et al. (TMS, Warrendale, 2008), pp. 191–200.